

The PANDA automatic weather station network between the coast and Dome A, East Antarctica

Minghu Ding¹, Xiaowei Zou^{1,2}, Qizhen Sun³, Diyi Yang¹, Wenqian Zhang¹, Lingen Bian¹, Changgui Lu¹, Ian Allison⁴, Petra Heil⁵, Cunde Xiao⁶

¹State Key Laboratory of Severe Weather, Chinese Academy of Meteorological Sciences, Beijing 100081, China

²GNSS research center, Wuhan University, Wuhan 430079, China

³Polar Research and Forecasting Division, National Marine Environmental Forecasting Center, Beijing 100081, China

⁴Institute for Marine and Antarctic Studies, University of Tasmania, Australia

⁵Australian Antarctic Division and Australian Antarctic Program Partnership,
University of Tasmania, Australia

⁶State Key Laboratory of Earth Surface Processes and Resource Ecology, Beijing Normal University, Beijing 100875, China

Correspondence to: Minghu Ding (dingminghu@foxmail.com) and Cunde Xiao (cdxiao@bnu.edu.cn)

Abstract: This paper introduces a unique multiyear dataset and the monitoring capability of the PANDA automatic weather station network which includes eleven automatic weather stations (AWS) across Prydz Bay-Amery Ice Shelf-Dome A area from the coast to the summit of the East Antarctica ice sheet. The ~1460 km transect from Zhongshan to Panda S follows roughly along $\sim 77^{\circ}$ E longitude and covers all geographic units of East Antarctica. Initial inland observations, near the coast, started in the 1996/1997 austral summer. All AWSs in this network measure air temperature, relative humidity, air pressure, wind speed and wind direction at 1-hour intervals, and some of them can also measure firn temperature and shortwave/longwave radiation. Data are relayed in near real-time via the ARGOS system. Data quality is generally very reliable and the data have been used widely. In this paper, we firstly present a detailed overview of the AWSs, including the sensor characteristics, installation procedure, data quality control protocol, and the basic analysis of each variable. We then give an example of a short-term atmospheric event that shows the monitoring capacity of the PANDA -AWS network. This dataset, which is publicly available, is planned to be updated on a near-real time and should be valuable for climate change estimation,

33 extreme weather events diagnosis, data assimilation, weather forecasting, etc. The
34 dataset is available at <https://doi.org/10.11888/Atmos.tpdc.272721> (Ding et al., 2022).

35 1. Introduction

36 Antarctica, covered by a vast ice sheet, has the coldest climate on Earth's surface
37 (Qin and Ren, 2001; Van den Broeke and Van Lipzig, 2003; Zhou et al., 2009). Great
38 efforts have been made to study Antarctic climate change under global warming
39 because of its role in the climate system and its capability to greatly impact global sea
40 level rise (IPCC, 2019; Huai et al., 2019). However, the reliability of Antarctic climate
41 change estimation and weather forecasting is still under debate (Hines et al., 2019;
42 Zhang et al., 2021). This is a consequence of the paucity of observations, especially at
43 long term inland weather stations, which can be directly assimilated in to models and
44 reanalysis data (Vignon et al., 2017; Wei et al., 2019).

45 The first attempt at automatic weather station (AWS) observations in Antarctica was
46 in 1956/57, when station XG1 was deployed by the United States near McMurdo; but
47 this station was short lived (Lazzara et al., 2012). Early attempts at AWS observations
48 were also made off the coast of East Antarctica by the Australian National Antarctic
49 Research Expedition (ANARE) at Chick Island (in 1961) and Lewis Island (in 1962).
50 Both these stations were also short lived.

51 Development of automatic observational technology in polar regions was greatly
52 advanced with initiation, in 1978, of the ARGOS data relay system on polar orbiting
53 satellites. This, together with more robust and power-efficient electronics, saw
54 successful Antarctic AWS deployments by the University of Wisconsin, USA,
55 commencing in 1980. The Australian Antarctic Division (AAD) also tested its design
56 of AWS at near-coastal sites in 1980 and deployed its first successful station on the
57 inland ice sheet, at 1830 m elevation, in January 1982 (Allison and Morrissey, 1983).
58 Subsequently, more and more Antarctic AWSs were installed: ~30 by 1990, ~55 by
59 2000, ~60 by 2010 and ~160 by 2020 (Bromwich et al., 2020). Many of these were
60 installed as part of a United States network on the Ross Ice Shelf, inland from the Adélie
61 Land coast for a study of katabatic wind flow, and at other interior ice sheet sites
62 (Lazzara et al., 2012). During the International Antarctic Glaciological Project traverses
63 from Casey station, of ANARE AWSs were deployed on the ice sheet, along about
64 110°E to 3096 m elevation. Australian glaciological traverses between Mawson and
65 Zhongshan deployed 5 AWSs at 2500 m elevation around the interior of the Lambert

66 Glacier Basin (LGB), between 1990 and 1994 (Allison et al., 1993; Allison, 1998; Heil,
67 2006). Further west in eastern Dronning Maud Land, stations were built and deployed
68 on the ice sheet by Japan at Dome Fuji (in December 1993) and Relay (in January 1993)
69 (Enomoto et al., 1995). To extend knowledge of the near-surface climate and heat budget
70 of Antarctica, Netherlands started to deploy AWSs in western Dronning Maud Land in
71 January 1997 (Reijmer and Oerlemans, 2002).

72 Several of the AWSs mentioned failed after a relatively short time, and those in high
73 accumulation near-coastal areas became buried by snow. But quite a few continued to
74 provide high-quality data for many years. For example, the Australian AWS at GC41,
75 inland of Casey at 2760 m elevation, provided good data for more than 21 years until
76 eventually buried, although it was never visited for maintenance. The interior ice sheet
77 with low accumulation, relatively low wind speeds, and no liquid water is a benign
78 environment for electronic systems if properly designed for very low temperatures. The
79 higher latitude sites also see more transits of polar-orbiting satellites carrying the
80 ARGOS data relay system.

81 These AWS observations have made valuable contributions to Antarctic research.
82 Firstly, the data have been used to evaluate weather and climate changes (Turner et al.,
83 2005; 2007; Wei et al., 2019; Wang et al., 2022). For example, Schwerdtfeger (1984)
84 gave a brief characterization of the inland Antarctica climate from AWS data. Allison
85 et al (1993) analyzed the influence of ice sheet topography on surface meteorology
86 using 10 AWSs from both the US-French network in Adélie Land and the Australian
87 network inland of Casey. Secondly, AWS data, including radiation measurements, can
88 be used to investigate ice/snow-atmosphere interaction processes in Antarctica. Van den
89 Broeke et al. (2004a; 2004b; 2005; 2006) studied the daily and seasonal variation of the
90 surface energy balance in detail in Dronning Maud Land. Ding et al. (2020; 2021a)
91 improved the surface energy balance simulation scheme at Dome A and the inland
92 Antarctic area with long term AWS measurements. Thirdly, AWS observations are also
93 critical in evaluating the applicability of reanalysis data and numerical models in
94 Antarctica. Nigro et al. (2011) estimated the performance of Antarctic Mesoscale
95 Prediction System (AMPS) under varied synoptic conditions with AWS data for the
96 Ross Ice Shelf. Xie et al (2014) assessed the accuracy of daily mean surface pressure
97 from different meteorological reanalyzes against in situ observations from automatic
98 weather stations in East Antarctica. Dong et al. (2020) evaluated the robustness of near-
99 surface wind speed of multiple global atmospheric reanalysis in Antarctica based on

100 many AWS and meteorological observations made at staffed stations. Recently, Wei et
101 al. (2019) and Turner et al. (2020) used multiple meteorological records to give the
102 spatial/temporal distribution of temperature extremes across Antarctica for the first time.

103 However, most staffed observational sites and AWSs in Antarctica are still mainly
104 located in the coastal area, and data from the sparse inland sites is interrupted frequently
105 (e.g., the anemometer was often frozen during austral winter at Eagle and Dome A)
106 (Wendler et al., 1988; Van As et al., 2005; Zhou et al., 2009; Lazzara et al., 2012; Sun
107 et al., 2018; Bromwich et al., 2020). More continuous and systematic AWS observation,
108 are still required from Antarctica.

109 Commencing in the 1996/1997 austral summer, the Chinese National Antarctic
110 Research Expedition (CHINARE) started deploying AWSs between the coastal
111 Zhongshan and inland Panda S (the PANDA transect). The first stations deployed on
112 this transect were manufactured by the AAD, but after 2012, the Chinese Academy of
113 Meteorological Sciences made great progress in AWS design, especially the ultra-low
114 temperature power supply system (patent for invention, Ding et al., 2021b), and
115 deployed 7 further AWSs along the PANDA transect.

116 Initial studies using these observations focused on the coastal area or a single site
117 (e.g., van den Broeke et al., 2004a; 2004b; Chen et al., 2010) while later studies used
118 data from more inland stations (Ma et al., 2010; Ding et al., 2021a). Only a few studies
119 have used meteorological information (shown in Table 1) from the whole transect (Zhou
120 et al. 2009; Ma et al. 2010; Bian et al. 2016). That is because only 5 of the initial AWSs
121 were still operating in 2012 (Dome A, Eagle, Panda N, Zhongshan and Panda S), others
122 had been buried by snow accumulation or failed due to low air temperature (Ding et al.,
123 2021a). Subsequent AWSs have been installed close to the locations of the failed
124 stations to extend the measurements (e.g., Panda 200 was installed close to LGB69).
125 The more recent deployments now provide consistent, high quality and real time
126 meteorological observations from the PANDA AWS network. Some data from the
127 PANDA AWS network have been compiled by WMO (e.g., Dome A ID: 89577, Eagle
128 ID: 89578, Kunlun ID: 89572, Taishan ID: 89576) and some are available as monthly
129 means from the Scientific Committee on Antarctic Research (SCAR) Reference
130 Antarctic Data for Environmental Research (READER)
131 (<https://www.bas.ac.uk/project/reader/>). But most of these data have not been published
132 before. Here, to promote and make available the value of these AWSs data, we provide
133 metadata of the dataset that will be updated in near-real time on the platform “Big Earth

134 Data for Three Poles" (<http://poles.tpdc.ac.cn/zh-hans/>). We also provide an overview
135 of the climate characteristics of the region.

136 **2 Observation region and data pre-processing**

137 2.1 Observation region and site descriptions

138 The PANDA transect is approximately along 77° E longitude, and stretches
139 approximately 1460 km from the coast at Zhongshan to the Dome A, region at the
140 summit of the East Antarctic Ice Sheet. This transect is highly representative of East
141 Antarctica for it covers Prydz Bay, Lambert Glacier/Amery Ice Shelf, high inland and
142 dome summit regions. According to Zhang et al. (2008) and Ding et al. (2011), the
143 PANDA transect can be divided into three typical topographies: a coastal region
144 characterized by steep terrain (corresponding to Zhongshan to Panda 200), an inland
145 region with strong katabatic wind (Panda 300 to Eagle), and a dome region (Panda 1100
146 to Panda S).

147 The PANDA AWS network had 11 AWSs in operation in 2022: Zhongshan, Panda
148 100, Panda 200 (LGB 69), Panda 300, Panda 400, Taishan, Eagle, Panda 1100, Dome
149 A, Kunlun and Panda S. All of them are located on the western side of the LGB (Fig.
150 1), at different latitudes (69° S-83° S) and at different elevations (detailed information
151 can be found in Table 1). The first site, Zhongshan was established in March 1989,
152 when CHINARE first arrived in East Antarctica (Zeng et al., 2021). It was initially a
153 Staffed Weather Station but has now been replaced by an AWS. LGB 69 (192 km from
154 the coast) was first deployed in January 2002 during the AAD Lambert Glacier Basin
155 traverse. This station was in a region of high ice velocity (17.7 m a⁻¹) and high
156 accumulation rate (199 kg m⁻² a⁻¹ for 2002-2003) (Zhang et al., 2008; Ma et al., 2010;
157 Ding et al., 2011; 2015) and it became buried approximately every 3 years, requiring
158 digging up and redeploying on the surface. It stopped operating by 2008 (Ding et al.,
159 2021a). Since it was difficult to maintain an AWS at the original site, PANDA 200 was
160 deployed 200 km from the coast in December 2016, and is considered as a replacement
161 AWS for LGB 69. In January 2005, Eagle and Dome A were installed during the
162 CHINARE 21st which reached the summit of East Antarctic Ice Sheet, ~1248 km from
163 the coast. Then in January 2008, Panda S was deployed in cooperation with the
164 University of Wisconsin as a contribution to the International Polar Year, but this AWS
165 has only operated intermittently. The other AWSs were manufactured by the Chinese
166 Academy of Meteorological Sciences and were deployed during 2012 (Taishan) and

167 2019 (Panda 100, Panda 300, Panda 400). The hourly data from the all AWSs are
168 remotely collected and relayed in near real-time by the ARGOS System. The data is not
169 stored internally.

170 It should be noted that these AWSs are of several different designs for different
171 scientific purposes. All include sensors for air temperature (T_a) and wind speed (WS),
172 initially at 1, 2, 4 and/or 6 m above surface, and wind direction (WD), relative humidity
173 (RH) and air pressure (P). Sensor height above the surface and station tilt are not part
174 of the monitored variables, and all sensor heights in this paper are the heights at initial
175 deployment. Panda 300, Taishan, Eagle and Dome A AWSs are also equipped with
176 surface and firn temperature probes (detailed information can be found in Table 1). The
177 Zhongshan is designed to WMO service regulation so the initial height of wind
178 measurement is 10 m.

179 The AWSs that were designed by the Chinese Academy of Meteorological Sciences
180 use a Vaisala HMP155 resistance probe to measure air temperature and relative
181 humidity. ~~Panda S use a Weed wire bridge and Vaisala HMP35A.~~ Eagle and Dome A
182 AWSs use FS23D thermistors and Vaisala HMP35D humidity probes (Xiao et al., 2008).
183 The Vaisala HMP155 is an integrated air temperature and relative humidity sensor, and
184 automatically accounts for whether RH is relative to water or ice. -The air pressure
185 sensor for Eagle and Dome A is a Paroscientific 6015A. Panda 100 and Taishan use
186 Vaisala PTB110 ~~and~~, Zhongshan and Panda S uses Campbell ~~Scientific~~ CS106 to
187 measure air pressure. ~~A Paroscientific Model 215A pressure sensor is used at Panda S,~~
188 and all other AWSs use Vaisala PTB210. Eagle and Dome A AWSs have cup
189 anemometers which freeze during extreme austral winter cold (Zhou et al., 2009; Ma
190 et al., 2010). The other AWSs are equipped with Huayun Zhongyi XFY3-1 wind
191 propeller anemometers and they are optimized to prevent “diamond dust” accumulation
192 on the instruments. Some stations (Panda 100, Panda 200, Panda 300, Panda 400,
193 Taishan, Panda 1100, Kunlun) also make radiation measurements. In addition, Panda
194 400, Taishan, Eagle and Panda 1100 use Campbell 109 to measure subsurface
195 temperature in different depth. These are not discussed in this paper, but are available
196 detailed and available for download from the data site. Further details of the sensor and
197 AWS schemes can be found in Table1.

198 All sensors are calibrated before the AWS deployment, but extremely cold weather
199 below -60 °C may bring uncertainty. The height of the sensors above surface gradually

200 decreases with snow accumulation. This has been ignored in the preliminary analysis
201 presented here.

202 2.2 Data quality control

203 All data are checked initially to ensure integrity, consistent with the approach of Ma
204 et al. (2010), Lazzara et al. (2012), and Wawrzyniak and Osuch (2020). A schematic
205 diagram of data processing workflow is shown in Figure 2. Firstly, ARGOS reception
206 may lead to duplicated records or time dislocation, these are removed. For those AWSs
207 with measurements of air temperature and wind speed at multiple levels, a check of the
208 vertical profiles is a particularly strong validation. If the vertical gradients are
209 physically consistent, then the absolute values are likely to be accurate. Secondly,
210 different variables are compared to check their consistency. For instance, wind direction
211 will be eliminated when wind speed is zero. In addition, the height of sensors might
212 change with snow accumulation. A correction method for this error has been introduced
213 in Ma et al. (2008) and Smeets et al. (2018). Daily mean values are averaged from
214 hourly data and then monthly and annual mean values are progressively calculated.
215 Similar to the methodology of Maturilli et al. (2013) and Zou et al. (2021), missing
216 values are handled depending on their duration. If more than 21% data (5 hours) during
217 one day, or 12% data (4 days) within one month, or 25% data (3 months) within one
218 year are missing, this daily/monthly/annual data is considered a missing value.

219 The measurements at Zhongshan were made only four times a day (00:00, 06:00,
220 12:00 and 18:00 UTC) from 1 March 1989 to 31 January 2002. Hence, we analyzed
221 diurnal data only from 2002 to 2020, but monthly and annual values from 1989 to 2020.
222 The average of meteorological variables at other AWSs were calculated for different
223 periods depending on their deployment dates, which are not the same (Table 1):
224 Panda100, Panda 300, Panda 400 and Panda 1100 span from 2019 to 2021; Panda 200
225 spans from 2016 to 2021; Taishan spans from 2012 to 2021; Eagle and Dome A span
226 from 2005 to 2020; Kunlun spans from 2017 to 2021; Panda S spans from 2008 to 2021.
227 All variables are analyzed at a height of 4 m, except at Zhongshan, Panda 200 and Panda
228 400. The wind speed and direction at Zhongshan are at 10 m, and the air temperature
229 and relative humidity at Panda 200 and Panda 1100 are at 6 m and 2 m, respectively.

230 Due to heavy hoar frost in the Antarctic inland, the anemometers with a vertical axis
231 at Eagle, Dome A and Panda S often froze during austral winter, which leads to invalid
232 measurements (Zhou et al., 2009). We used a different type of anemometer on the other
233 AWSs and deleted the wintertime wind speed and direction data for these three AWSs.

234 **3 Results**

235 **3.1 Air temperature**

236 The mean diurnal variation of air temperature is approximately sinusoidal curve at
237 all AWSs (Fig. 3). The maximum air temperature occurs at 0900-1100 UTC (1400-1600,
238 Local Solar Time LST), and the minimum was at 2200-2300 UTC (0300-0400, LST).
239 From the coast to the dome area, the standard deviation of diurnal variations gradually
240 increases (from 0.64 °C at Zhongshan to 1.42 °C at Panda S), consistent with the result
241 of King et al. (2006). This regularity may be the result of katabatic wind, marine effect
242 and cloud (van den Broeke, et al., 2004a; Zhou et al., 2008).

243 The monthly mean air temperatures, particularly for the more southern AWSs, show
244 a “coreless” winter with a single “valley” pattern; in other words, there is no distinctive
245 minimum during austral winter (Fig. 4) (Allison et al., 1993; Chen et al., 2010; Ma et
246 al., 2010). The variability (standard deviation of monthly air temperature) in austral
247 winter is much larger than in austral summer, e.g., 2.46 °C vs 1.67 °C at Taishan. This
248 indicates that the Antarctic Ice Sheet experiences more weather activities during austral
249 winter. For example, sometime cyclones from the surrounding ocean may bring warm,
250 moist air masses (Qin et al., 2017; Ding et al., 2020). In addition, the inland region
251 exhibits more dynamic weather than either the coast or the dome summit regions,
252 coinciding with a larger standard deviation in monthly air temperature. This is 1.5 times
253 (3.24 °C) that of the others two regions (2.19 °C, and 2.39 °C respectively).

254 With consideration of the length of the observation period, the trend in annual mean
255 air temperatures is shown for only 4 AWSs in Fig. 5. These are Zhongshan (1989 to
256 2020), Taishan (2013 to 2020), Eagle (2005 to 2020) and Dome A (2005 to 2020). They
257 have annual means of -10.0 °C, -35.4 °C, -41.2 °C and -50.4 °C respectively, like the
258 results of Ma et al. (2010). This difference can be attributed to differences in
259 elevation/topography and latitude (Allison et al., 1993).

260 **3.2 Relative humidity**

261 The variation of local atmospheric moisture is driven by a combination of large-scale
262 advection and local evaporation/sublimation effects (Maturilli et al., 2013). Figure 6
263 shows a similar distribution to a previous study (Ma et al., 2010); the austral summer is
264 more humid than the austral winter at all AWSs. However, coastal relative humidity
265 fluctuates largely on the monthly scale but there is a little difference between austral
266 summer and winter. At the inland and dome summit regions, the monthly relative

267 humidity has a very clear seasonal cycle (except Dome A).

268 Figure 7 shows the annual averages and trends of relative humidity at Zhongshan,
269 Taishan, Eagle and Dome A. Relative humidity varied considerably at all sites, with the
270 driest records at Dome A. Interestingly, the relative humidity is well correlated with air
271 temperature except at Zhongshan, partially because its weather is controlled by the
272 adjacent ocean.

273 3.3 Air Pressure

274 Air pressure obviously decreases with elevation from coast to dome area, and the
275 seasonal cycle becomes clearer. Monthly mean air pressure shows a semi-annual
276 oscillation with equinoctial minima near the coastal and inland areas along the PANDA
277 AWS network, but is much less distinct at the dome area. The semi-annual oscillation
278 there could be hidden under larger annual oscillation (Fig. 8) (Radok et al., 1996).
279 Coastal areas like Zhongshan, Panda 100 and Panda 200 have little air pressure
280 difference between austral summer and winter, but there are obvious differences for the
281 inland area, with a stable-strong low-pressure structure at the plateau surface in austral
282 winter. However, there is more cyclonic activity in the inland area (Panda 300 to Eagle)
283 (Ding et al., 2020). This is shown by the highest standard deviation of air pressure, (705 ± 4 hPa),
284 higher than the coastal (858 ± 3.10 hPa) and the dome areas (585 ± 2.74 hPa).
285 The annual averages (Table 2) and trend of air pressure at the AWS shows no systematic
286 variation, consistent with Zhou et al. (2009) and most other studies in East Antarctica.

287 3.4 Wind speed and direction

288 Diurnal variation in wind speed shows most clearly in the coastal katabatic region
289 (Fig. 9). The maximum wind speed occurs around 0400-0800 UTC (0900-1300 LST)
290 and the minimum around 1400-1600 UTC (1900-2100 LST) at near-coastal AWSs.
291 Diurnal variation of wind speed gradually decreases from the coast to the dome region,
292 from Panda 1100 to Panda S. Panda S showed very weak fluctuation because the dome
293 area is a sink center for atmosphere circulation and the origin of Antarctic surface wind
294 flow (Parish and Bromwich, 1987; Van den Broeke and Van Lipzig, 2003; Aristidi et
295 al., 2005; Das et al., 2013). This phenomenon is also reflected in the vertical
296 temperature gradient difference. At all times of day, the surface atmosphere has a
297 positive temperature gradient (the 4 m air temperature is higher than 2 m). Thus, the
298 wind is weak and wind direction is stable at Dome A. Similarly, Zhou et al. (2009) and

299 Bian et al. (2016) also found that there was a persistent and stable inversion layer due
300 to strong surface cooling of the Antarctic Ice Sheet.

301 There is evidence of seasonal variations of wind speed at all AWSs except Eagle,
302 Dome A and Panda S. The austral winter wind speed is higher than austral summer (Fig.
303 10). This is related to the intensity of surface cooling and topography of the ice sheet.
304 Wind flow can be accelerated by cooling along a slope (Van den Broeke et al., 2002).
305 The fluctuation of wind speed was much greater in austral winter than in summer, e.g.,
306 the standard deviations at Panda 200 in austral winter and summer were 1.43 m s^{-1} and
307 0.99 m s^{-1} respectively. From the coast to dome area, the wind speed decreased, which
308 has also been discussed by Ma and Bian (2014) and can be attributed to the katabatic
309 wind effect. Zhongshan is an exception: its wind speed is weaker than at the other
310 coastal AWSs. This AWS was deployed on rock more than 2 km from the edge of the
311 ice sheet where the katabatic wind has weakened.

312 Over the long-term, the wind speed showed a weakening trend over the whole
313 transect (Fig. 11). The trend at Zhongshan was $-0.41 \text{ m s}^{-1}/\text{decade}$ ($p < 0.01$) from 1989
314 to 2020. This phenomenon deserves future investigation.

315 As has been previously noted, the vertical axis anemometers of Dome A and Eagle
316 are often frozen during austral winter, and the data quality of wind during austral fall is
317 poor. Therefore, we only analyzed wind direction for the months from September to
318 February at these two sites. Figure 1 showed the wind rose distribution of all AWSs.
319 The wind directions at coastal and inland areas (from Zhongshan to Taishan) were
320 relatively regular: during austral summer, constant easterlies determine the wind speed
321 on the ice sheet. In austral winter, katabatic forcing from strong surface cooling, large-
322 scale pressure gradient and Coriolis force, dominates, also resulting in winds from NE
323 to SE (Van den Broeke et al., 2002; Van den Broeke and Van Lipzig, 2003). At the dome
324 summit region, the wind direction has a broad distribution with weak wind speed south,
325 southeast and west. At Dome A, 16 years of observations show no prevailing wind
326 direction.

327 **4. Capability of monitoring short-term atmospheric events**

328 Compared to other meteorological observations, one advantage of the PANDA AWS
329 network is that it covers all terrain and climatic sectors of East Antarctica. The local
330 weather conditions can be deduced from the meteorological surface measurements.
331 Figure 12 shows the course of air pressure, air temperature, relative humidity and wind

332 speed from 30th July to 3rd August 2020, which indicates the occurrence of a prominent
333 blocking event. To assess the capability to monitor weather conditions, this physical
334 atmospheric process was analyzed using the PANDA AWSs network dataset.

335 On 1st August 2020, the blocking stretched southward to around 100° E, forming a
336 high-pressure ridge in the interior of ice sheet (Fig. 13). The deep low-pressure system
337 was blocked from moving eastward and thus stagnated near Prydz Bay. This situation
338 facilitated the meridional advection of warm, moist air masses. It can be seen in Fig.
339 12, that the air temperature, relative humidity, air pressure and wind speed from
340 Zhongshan to Dome A changed with the development of the event. The uppermost site
341 to detect the blocking is Dome A at 4093 m a.s.l. and the average speed of the blocking
342 event across transect was about 40 km/h. Before 1st August, there was a drastic drop in
343 air pressure at AWSs from Zhongshan to Taishan, reaching the lowest value at local
344 noon, but the air pressure from Eagle to Dome A showed no such changes. Meanwhile,
345 the air temperature, relative humidity and wind speed show the opposite change at all
346 AWSs, rising sharply and reaching the highest values at local noon, indicative of
347 maritime air intrusions to the PANDA transect. On 3 August, the deep low-pressure
348 system was slightly weaker (not shown). The southern section of the Indian Ocean
349 subtropical high became weak in the geopotential height anomaly field, and the
350 blocking event moved eastward and eventually dissipated along the coast. This event
351 was like a recent abrupt warming event at Dome C (Ding et al., 2022a). Therefore, the
352 PANDA AWS network provides high spatial-temporal observations and can play an
353 important role in the mesoscale circulation research on the Antarctic Ice Sheet.

354 **5. Data availability**

355 This dataset is publicly available and it is planned that it will be updated on a near-
356 real time. The data from all AWSs will be publicly available on the platform “Big Earth
357 Data for Three Poles”. The links are as follows: Zhongshan, Panda 100, Panda 200,
358 Panda 300, Panda 400, Taishan, Panda 1100 and Kunlun, the data can be downloaded
359 from <https://doi.org/10.11888/Atmos.tpdc.272721> (Ding et al., 2022b). Eagle and
360 Dome A data has been published on the data portal of AAD:
361 <http://aws.cdaso.cloud.edu.au/datapage.html>. Panda S data has been posted on the data
362 portal of the University of Wisconsin: <https://doi.org/10.48567/1hn2-nw60> (AMRDC
363 Data Repository).

364 **6. Conclusion**

365 In this paper, we have introduced the PANDA AWS network which can monitor the
366 meteorology from the coastal Zhongshan AWS to Panda S in the interior of the
367 Antarctic continent with high spatial and temporal resolution. The data collected during
368 the past decades are reliable after calibration and homogenization, and have been used
369 widely in meteorological and climate change research in Antarctica (e.g., Xie et al.,
370 2016, Ding et al. 2021a). The data can also be used to assimilated into reanalyzes, and
371 used to evaluate climate models and to validate satellite data.

372 In a preliminary analysis, the diurnal, monthly, annual averages as well as long term
373 changes have been presented. They show distinct differences between coastal, inland
374 and dome summit regions. An example has also been given of a short-term atmospheric
375 process to show this dataset's capability for weather monitoring and investigating.

376 **Author contributions.**

377 MD, IA and XZ designed the experiments and wrote the manuscript; MD carried out
378 the experiments; XZ and DY analyzed the experimental results. MD, XZ, PH and DY
379 revised the manuscript; CL, QS and WZ provides the information of AWS; DY, LB and
380 CX discussed the results.

381 **Competing interests.**

382 The authors declare that they have no conflict of interest.

383 **Acknowledgements.**

384 The observations and AWS deployments were carried out during the Chinese
385 National Antarctic Research Expedition from Zhongshan to Kunlun. We are grateful to
386 David Mikolajczyk from Antarctic Meteorological Research and Data Center at the
387 University of Wisconsin for providing meteorological data and AWS information for
388 Panda S.

389 **Financial support.**

390 This research has been supported by the National Science Foundation of China
391 (42122047), the National Key Research and Development Program of China
392 (2021YFC2802504) and Basic fund of CAMS (2021Z006).

393

394 **Reference**

395 Allison, I. and Morrissy, J.V.: Automatic weather stations in Antarctica. Australian
396 Meteorological Magazine, 31(2),71-76, 1983.

397 Allison, I., Wendler, G., and Radok, U.: Climatology of the East Antarctic ice sheet
398 (100°E to 140°E) derived from automatic weather stations, Journal of Geophysical
399 Research: Atmospheres, 98(D5), 8815-8823, <https://doi.org/10.1029/93JD00104>,
400 1993.

401 Allison, I. Surface climate of the interior of the Lambert Glacier basin, Antarctica, from
402 automatic weather station data. Annals of Glaciology, 27, 515-520.
403 <https://doi.org/10.3189/1998AoG27-1-515-520>, 1998.

404 Antarctic Meteorological Research and Data Center: Automatic Weather Station
405 quality-controlled observational data. AMRDC Data Repository. Subset used:
406 [DATE 1]-[DATE 2], accessed DD-MM-YYYY, <https://doi.org/10.48567/1hn2-nw60>.

408 Aristidi, E., Agabi, K., Azouit, M., Fossat, E., Vernin, J., Travouillon, T., Lawrence, J.
409 S., Meyer, C., Storey, J. W. V., Halter, B., Roth, W. L., and Walden, V.: An analysis
410 of temperatures and wind speeds above Dome C, Antarctica. Astronomy &
411 Astrophysics, 430(2), 739-746, <https://doi.org/10.1051/0004-6361:20041876>, 2005.

412 Bian, L., Allison, I., Xiao, C., Ma, Y., Fu, L., and Ding, M.: Climate and meteorological
413 processes of the East Antarctic ice sheet between Zhongshan and Dome-A, Advances
414 in Polar Science, 27(2), 90-101, <https://doi.org/10.13679/j.advps.2016.2.00090>,
415 2016.

416 Bromwich, D. H., Werner, K., Casati, B., Powers, J. G., Gorodetskaya, I. V., Massonnet,
417 F., Vitale, V., Heinrich, V. J., Liggett, D., Arndt, S., Barja, B., Bazile, E., Carpentier,
418 S., Carrasco, J. F., Choi, T., Choi, Y., Colwell, S. R., Cordero, R. R., Gervasi, M.,
419 Haiden, T., Hirasawa, Na., Inoue, J., Jung, T., Kalesse, H., Kim, S.J., Lazzara, M. A.,
420 Manning, K. W., Norris, K., Park, S. J., Reid P., Rigor, I., Rowe, P. M., Schmithüsen,
421 H., Seifert, P., Sun, Q., Uttal, T., Zannoni, M., and Zou, X.: The Year of Polar
422 Prediction in the Southern Hemisphere (YOPP-SH), Bulletin of the American
423 Meteorological Society, 101(10), E1653-E1676, <https://doi.org/10.1175/BAMS-D-19-0255.1>, 2020.

425 Chen, B., Zhang, R., Xiao, C., Bian, L., and Zhang, T.: Analyses on the air and snow
426 temperatures near ground with observations of an AWS at Dome A, the summit of

427 Antarctic Plateau, Chinese Science Bulletin, 55(11), 1048-1054,
428 <https://doi.org/10.1007/s11434-010-0099-1>, 2010.

429 Das, I., Bell, R. E., Scambos, T. A., Wolovick, M., Creyts, T. T., Studinger, M., Frearson,
430 N., Nicolas, J. P., Lenaerts, J. T. M., and Van Den Broeke, M. R.: Influence of
431 persistent wind scour on the surface mass balance of Antarctica. *Nature Geoscience*,
432 6(5), 367-371 <https://doi.org/10.1038/ngeo1766>, 2013.

433 Ding, M., Xiao, C., Li, Y., Ren, J., Hou, S., Jin, B., and Sun, B.: Spatial variability of
434 surface mass balance along a traverse route from Zhongshan station to Dome A,
435 Antarctica, *Journal of Glaciology*, 57(204), 658-666,
436 <https://doi.org/10.3189/002214311797409820>, 2011.

437 Ding, M., Xiao, C., Li, C., Qin, D., Jin, B., Shi, G., Xie, A., and Cui, X.: Surface mass
438 balance and its climate significance from the coast to Dome A, East Antarctica,
439 *Science China Earth Sciences*, 58(10), 1787-1797, <https://doi.org/10.1007/s11430-015-5083-9>, 2015.

440 Ding, M., Yang, D., Van den Broeke, M. R., Allison, I., Xiao, C., Qin, D., and Huai, B.:
441 The surface energy balance at Panda 1 station, Princess Elizabeth Land: A typical
442 katabatic wind region in East Antarctica, *Journal of Geophysical Research: Atmospheres*,
443 125(3), e2019JD030378, <https://doi.org/10.1029/2019JD030378>,
444 2020.

445 Ding, M., Zhang, T., Yang, D., Allison, I., Dou, T., and Xiao, C.: Brief communication:
446 Evaluation of multiple density-dependent empirical snow conductivity relationships
447 in East Antarctica, *Cryosphere*, 15, 4201-4206, <https://doi.org/10.5194/tc-15-4201-2021a>.

448 Ding, M., Du, F., Zhang, W., Wen, H., and Lu, C.: Battery system adapted to polar ultra-
449 low temperature environment and its temperature control method, Beijing:
450 CN113659246A, 2021b.

451 Ding, M., Xiao, C., and Qin, D.: Explosive warming event in Antarctica on 18 March
452 2022 and its possible causes. *Advances in Climate Change Research*,
453 <https://doi.org/10.12006/j.issn.1673-1719.2022.068>, 2022a.

454 Ding, M., Zou, X., Sun, Q., Yang, D., Zhang, W., Bian, L., Lu, C., Allison, I., Heil, P.,
455 and Xiao, C.: The PANDA automatic weather station network between the coast and
456 Dome A, East Antarctica (1989-2021). A Big Earth Data Platform for Three Poles,
457 <https://doi.org/10.11888/Atmos.tpdc.272721>, 2022b.

458 Dong, X., Wang, Y., Hou, S., Ding, M., Yin, B., and Zhang, Y.: Robustness of the recent
459

461 global atmospheric reanalyses for Antarctic near-surface wind speed climatology,
462 Journal of Climate, 33(10), 4027-4043, <https://doi.org/10.1175/JCLI-D-19-0648.1>,
463 2020.

464 Enomoto, H., Warashina, H., Motoyama, H., Takahashi, S., and Koike, J.: Data-logging
465 automatic weather station along the traverse route from Syowa Station to Dome Fuji,
466 Proc. of the NIPR Symp. on Polar Meteorol. and Glaciol., 9, 66-75,
467 <https://doi.org/10.15094/00003880>, 1995.

468 Heil, P.: Atmospheric conditions and fast ice at Davis, East Antarctica: A case study.
469 Journal of Geophysical Research: Oceans, 111(C5),
470 <https://doi.org/10.1029/2005JC002904>, 2006.

471 Hines, K. M., Bromwich, D. H., Wang, S. H., Silber, I., Verlinde, J., and Lubin, D.:
472 Microphysics of summer clouds in central West Antarctica simulated by the Polar
473 Weather Research and Forecasting model (WRF) and the Antarctic Mesoscale
474 Prediction System (AMPS), Atmospheric Chemistry and Physics, 19(19), 12431-
475 12454, <https://doi.org/10.5194/acp-19-12431-2019>, 2019.

476 Huai, B., Wang, Y., Ding, M., Zhang, J., and Dong, X.: An assessment of recent global
477 atmospheric reanalyses for Antarctic near surface air temperature, Atmospheric
478 Research, 226, 181-191, <https://doi.org/10.1016/j.atmosres.2019.04.029>, 2019.

479 Intergovernmental Panel on Climate Change.: IPCC special report on the ocean and
480 cryosphere in a changing climate, <https://archive.ipcc.ch/srocc/>, 2019.

481 King, J. C., Argentini, S. A., and Anderson, P. S.: Contrasts between the summertime
482 surface energy balance and boundary layer structure at Dome C and Halley stations,
483 Antarctica. Journal of Geophysical Research: Atmospheres, 111(D2),
484 <https://doi.org/10.1029/2005JD006130>, 2006.

485 Lazzara, M. A., Weidner, G. A., Keller, L. M., Thom, J. E., and Cassano, J. J.: Antarctic
486 automatic weather station program: 30 years of polar observation, Bulletin of the
487 American Meteorological Society, 93(10), 1519-1537, <https://doi.org/10.1175/BAMS-D-11-00015.1>, 2012.

489 Ma, Y., Bian, L., Xiao, C., Allison, I.: Correction of snow accumulation impacted on
490 air temperature from automatic weather station on the Antarctic Ice Sheet. Advance
491 in Polar Science, 20(04): 299-309, <http://ir.casnw.net/handle/362004/7877>, 2008.

492 Ma, Y., Bian, L., Xiao, C., Allison, I., and Zhou, X.: Near surface climate of the traverse
493 route from Zhongshan Station to Dome A, East Antarctica, Antarctic Science, 22(4),
494 443-459, <https://doi.org/10.1017/S0954102010000209>, 2010.

495 Ma, Y., and Bian, L.: A Surface Climatological Validation of ERA-interim Reanalysis
496 and NCEP FNL Analysis over East Antarctic, Chinese Journal of Polar Research,
497 26(4), 469-480, <https://doi.org/10.13679/j.jdyj.2014.4.469>, 2014.

498 Maturilli, M., Herber, A., and König-Langlo, G.: Climatology and time series of surface
499 meteorology in Ny-Ålesund, Svalbard, Earth System Science Data, 5(1), 155-163,
500 <https://doi.org/10.5194/essd-5-155-2013>, 2013.

501 Nigro, M. A., Cassano, J. J., and Seefeldt, M. W.: A weather-pattern-based approach to
502 evaluate the Antarctic Mesoscale Prediction System (AMPS) forecasts: Comparison
503 to automatic weather station observations, Weather and Forecasting, 26(2), 184-198,
504 <https://doi.org/10.1175/2010WAF2222444.1>, 2011.

505 Parish, T., and Bromwich, D.: The surface wind-field over the Antarctic ice sheets,
506 Nature 328, 51-54, <https://doi.org/10.1038/328051a0>, 1987.

507 Qin, D., and Ren, J.: The Antarctic Glaciology, Science Press, 2001.

508 Qin, T., Wei, L., and Ling, C.: The statistic and variance of cyclones enter in scientific
509 investigation station of China in Antarctic, Acta. Oceanologica Sinica, 39(5), 44-60,
510 <https://doi.org/10.3969/j.issn.0253-4193.2017.05.005>, 2017.

511 Radok, U., Allison, I. and Wendler, G.: Atmospheric surface pressure over the interior
512 of Antarctica. Antarctic Science, 8(2), 209-217, 1996.

513 Reijmer, C. H., and Oerlemans, J.: Temporal and spatial variability of the surface energy
514 balance in Dronning Maud Land, East Antarctica, Journal of Geophysical Research:
515 Atmospheres, 107(D24), ACL-9, <https://doi.org/10.1029/2000JD000110>, 2002.

516 Schwerdtfeger, W.: Weather and climate of the Antarctic, New York: Elsevier Science,
517 1984.

518 Smeets, P. C., Kuipers Munneke, P., Van As, D., van den Broeke, M. R., Boot, W.,
519 Oerlemans, H., Snellen, H., Reijmer, C.H., and van de Wal, R. S.: The K-transect in
520 west Greenland: Automatic weather station data (1993-2016), Arctic, Antarctic, and
521 Alpine Research, 50(1), S100002, <https://doi.org/10.1080/15230430.2017.1420954>,
522 2018.

523 Sun, Q. Z., Zhang, L., Meng, S., Shen, H., Ding, Z. M., and Zhang, Z. H.:
524 Meteorological observations and weather forecasting services of the CHINARE, Adv
525 Polar Sci, 28 (4), 291-299, <https://doi.org/10.13679/j.advps.2018.4.00291>, 2018.

526 Turner, J., Colwell, S. R., Marshall, G. J., Lachlan-Cope, T. A., Carleton, A. M., Jones,
527 P. D., Lagun V., Reid P. A., and Iagovkina, S.: Antarctic climate change during the
528 last 50 years, International Journal of Climatology, 25(3), 279-294,

529 <https://doi.org/10.1002/joc.1130>, 2005.

530 Turner, J., Overland, J. E., and Walsh, J. E.: An Arctic and Antarctic perspective on
531 recent climate change, *International Journal of Climatology: A Journal of the Royal*
532 *Meteorological Society*, 27(3), 277-293, <https://doi.org/10.1002/joc.1406>, 2007.

533 Turner, J., Marshall, G. J., Clem, K., Colwell, S., Phillips, T., and Lu, H.: Antarctic
534 temperature variability and change from station data. *International Journal of*
535 *Climatology*, 40(6), 2986-3007, <https://doi.org/10.1002/joc.6378>, 2020.

536 Van As, D., Van den Broeke, M. R., and Van De Wal, R.: Daily cycle of the surface
537 layer and energy balance on the high Antarctic Plateau, *Antarctic Science*, 17(1), 121-
538 133, <https://doi.org/10.1017/S095410200500252X>, 2005.

539 Van den Broeke, M. R., Van Lipzig, N. P. M., and Van Meijgaard, E.: Momentum budget
540 of the East Antarctic atmospheric boundary layer: Results of a regional climate model,
541 *Journal of the Atmospheric Sciences*, 59(21), 3117-3129,
542 [https://doi.org/10.1175/1520-0469\(2002\)059<3117:MBOTEA>2.0.CO;2](https://doi.org/10.1175/1520-0469(2002)059<3117:MBOTEA>2.0.CO;2), 2002.

543 Van den Broeke, M. R., and Van Lipzig, N. P. M.: Factors controlling the near-surface
544 wind field in Antarctica, *Monthly Weather Review*, 131(4), 733-743,
545 [https://doi.org/10.1175/1520-0493\(2003\)131<0733:FCTNSW>2.0.CO;2](https://doi.org/10.1175/1520-0493(2003)131<0733:FCTNSW>2.0.CO;2), 2003.

546 Van den Broeke, M. R., Reijmer, C. H., and Van De Wal, R.: Surface radiation balance
547 in Antarctica as measured with automatic weather stations, *Journal of Geophysical*
548 *Research: Atmospheres*, 109(D9), <https://doi.org/10.1029/2003JD004394>, 2004a.

549 Van den Broeke, M. R., Reijmer, C. H., and Van De Wal, R. S.: A study of the surface
550 mass balance in Dronning Maud Land, Antarctica, using automatic weather stations,
551 *Journal of Glaciology*, 50(171), 565-582,
552 <https://doi.org/10.3189/172756504781829756>, 2004b.

553 Van den Broeke, M. R., Reijmer, C. H., Van As, D., Van de Wal, R., and Oerlemans, J.:
554 Seasonal cycles of Antarctic surface energy balance from automatic weather stations,
555 *Annals of Glaciology*, 41, 131-139, <https://doi.org/10.3189/172756405781813168>,
556 2005.

557 Van Den Broeke, M. R., Reijmer, C. H., Van As, D., and Boot, W.: Daily cycle of the
558 surface energy balance in Antarctica and the influence of clouds, *International*
559 *Journal of Climatology: A Journal of the Royal Meteorological Society*, 26(12),
560 1587-1605, <https://doi.org/10.1002/joc.1323>, 2006.

561 Vignon, E., Genthon, C., Barral, H., Amory, C., Picard, G., Gallée, H., Casasanta, G.,
562 and Argentini, S.: Momentum-and heat-flux parametrization at Dome C, Antarctica:

563 A sensitivity study, *Boundary-Layer Meteorology*, 162(2), 341-367,
564 <https://doi.org/10.1007/s10546-016-0192-3>, 2017.

565 Wang, S., Ding, M., Liu, G., Wei, T., Zhang, W., Chen, W., Dou, T., and Xiao, C.: On
566 the Drivers of Temperature Extremes on the Antarctic Peninsula During Austral
567 Summer, *Climate Dynamics*, <https://doi.org/10.1007/s00382-022-06209-0>, 2022.

568 Wawrzyniak, T., and Osuch, M.: A 40-year High Arctic climatological dataset of the
569 Polish Polar Station Hornsund (SW Spitsbergen, Svalbard), *Earth System Science
570 Data*, 12(2), 805-815, <https://doi.org/10.5194/essd-12-805-2020>, 2020.

571 Wei, T., Yan, Q., and Ding, M.: Distribution and temporal trends of temperature
572 extremes over Antarctica, *Environmental Research Letters*, 14(8), 084040,
573 <https://doi.org/10.1088/1748-9326/ab33c1>, 2019.

574 Wendler, G., Ishikawa, N., and Kodama, Y.: The heat balance of the Icy slope of Adelie
575 Land, Eastern Antarctica, *Journal of Applied Meteorology*, 27(1), 52-65,
576 [https://doi.org/10.1175/1520-0450\(1988\)027<0052:THBOTI>2.0.CO;2](https://doi.org/10.1175/1520-0450(1988)027<0052:THBOTI>2.0.CO;2), 1988.

577 Xiao, C., Li, Y., Allison, I., Hou, S., Dreyfus, G., Barnola, J. M., Ren, J., Bian, L., Zhang,
578 S., and Kameda, T.: Surface characteristics at Dome A, Antarctica: first
579 measurements and a guide to future ice-coring sites, *Annals of Glaciology*, 48, 82-
580 87, <https://doi.org/10.3189/172756408784700653>, 2008.

581 Xie, A., Allison, I., Xiao, C., Wang, S., Ren, J., and Qin, D.: Assessment of surface
582 pressure between Zhongshan and Dome A in East Antarctica from different
583 meteorological reanalyses. *Arctic, Antarctic, and Alpine Research*, 46(3), 669-681,
584 <https://doi.org/10.1657/1938-4246-46.3.669>, 2014.

585 Xie, A., Wang, S., Xiao, C., Kang, S., Gong, J., Ding, M., Li, C., Dou, T., Ren, J., and
586 Qin, D.: Can temperature extremes in East Antarctica be replicated from ERA Interim
587 reanalysis? *Arctic, Antarctic, and Alpine Research*, 48(4), 603-621,
588 <https://doi.org/10.1657/AAAR0015-048>, 2016.

589 Zeng, Z., Wang, Z., Ding, M., Zheng, X., Sun, X., Zhu, W., Zhu, K., An, J., Zang, L.,
590 Guo, J., and Zhang, B.: Estimation and Long-term Trend Analysis of Surface Solar
591 Radiation in Antarctica: A Case Study of Zhongshan Station. *Advances in
592 Atmospheric Sciences*, 38(9), 1497-1509, <https://doi.org/10.1007/s00376-021-0386-6>, 2021.

594 Zhang, S., E, D., Wang, Z., Li, Y., Jin, B., and Zhou, C.: Ice velocity from static GPS
595 observations along the transect from Zhongshan station to Dome A, East Antarctica,
596 *Annals of Glaciology*, 48, 113-118, <https://doi.org/10.3189/172756408784700716>,

597 2008.

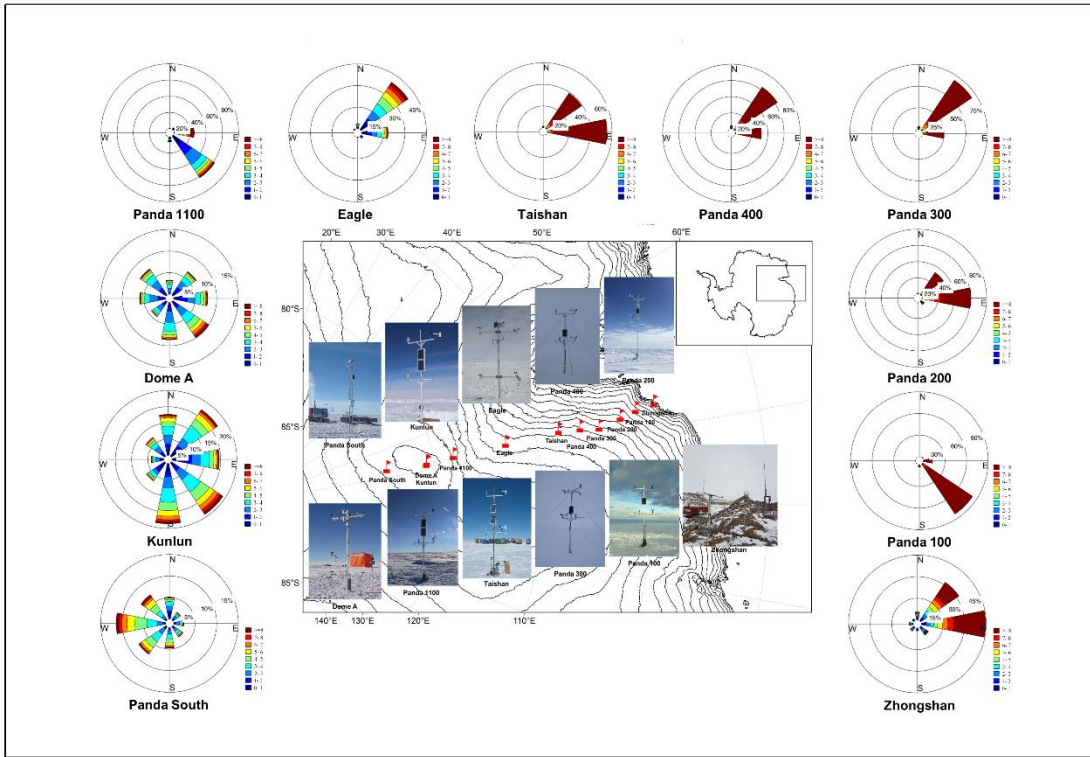
598 Zhang, Y., Wang, Y., and Hou, S.: Reliability of Antarctic air temperature changes from
599 Polar WRF: A comparison with observations and MAR outputs, *Atmospheric*
600 *Research*, 105967, <https://doi.org/10.1016/j.atmosres.2021.105967>, 2021.

601 Zhou, M., Zhang, Z., Zhong, S., Lenschow, D., Hsu, H. M., Sun, B., Gao, Z., Li, S.,
602 Bian, X., and Yu, L.: Observations of near-surface wind and temperature structures
603 and their variations with topography and latitude in East Antarctica, *Journal of*
604 *Geophysical Research: Atmospheres*, 114(D17),
605 <https://doi.org/10.1029/2008JD011611>, 2009.

606 Zou, X., Ding, M., Sun, W., Yang, D., Liu, W., Huai, B., Jin, S., and Xiao, C.: The
607 surface energy balance of Austre Lovénbreen, Svalbard, during the ablation period
608 in 2014, *Polar Research*, 40, <https://doi.org/10.33265/polar.v40.5318>, 2021.

609

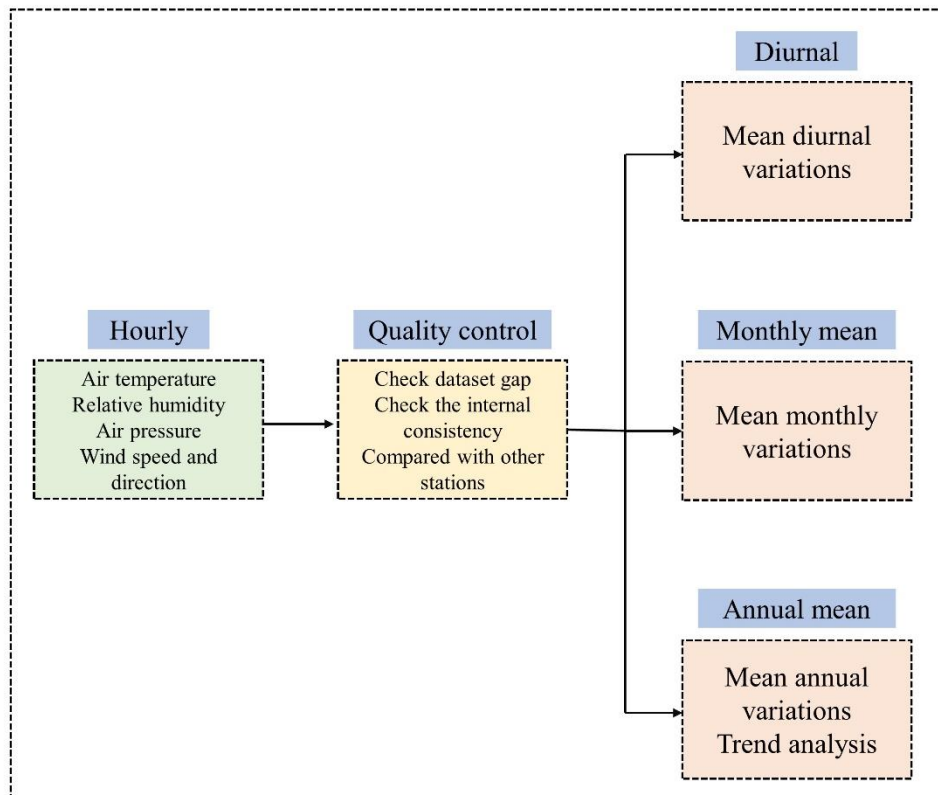
610 **Figures and Table:**



611

612 Figure 1. The location and Wind roses of AWSs in the PANDA network. The red flags
 613 are AWSs; the black solid lines are 200 m interval contours. The wind directions are
 614 divided into 22.5° sectors. Zhongshan is calculated during 1989-2020; Panda 100,
 615 Panda 300 and Panda 400 are calculated during 2019-2021; Panda 200 is calculated
 616 during 2016-2021; Taishan is calculated during 2012-2021; Eagle and Dome A are
 617 calculated during 2005-2020; Kunlun is calculated during 2017-2021; and Panda S is
 618 calculated during 2008-2021. Note however that, because some winter data were
 619 unreliable, Eagle averages exclude Mar-Aug; Dome A averages exclude March-
 620 October; and Panda S averages exclude May-September.

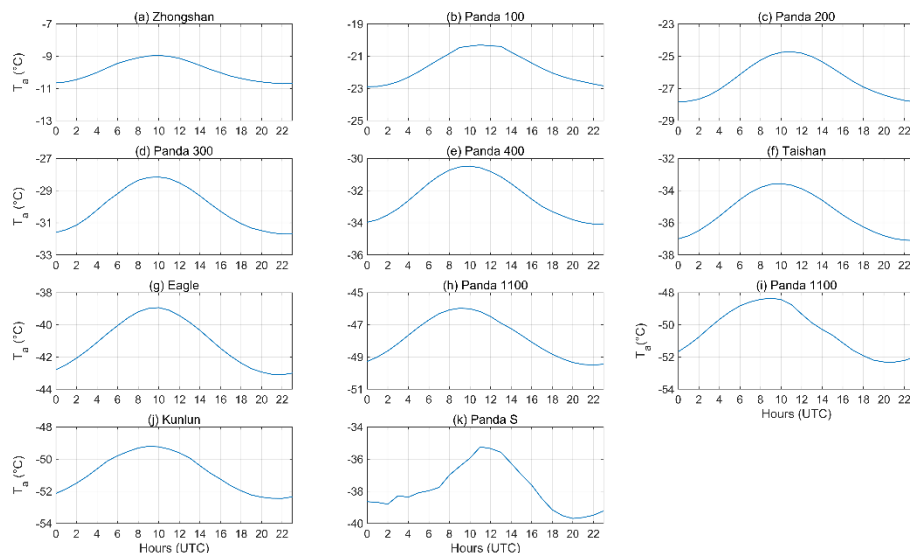
621



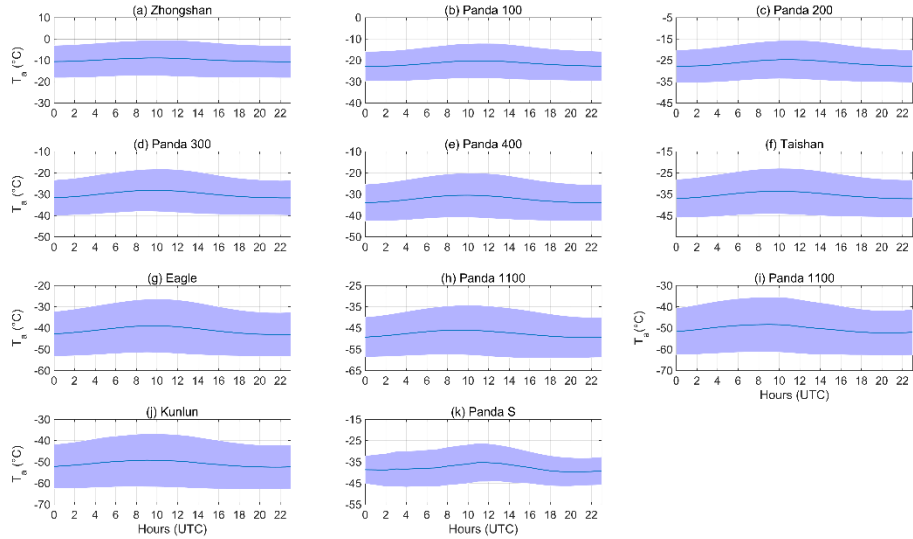
622

623 Figure 2. Schematic diagram of data processing workflow used to compile the AWS
 624 meteorology dataset for the network.

625



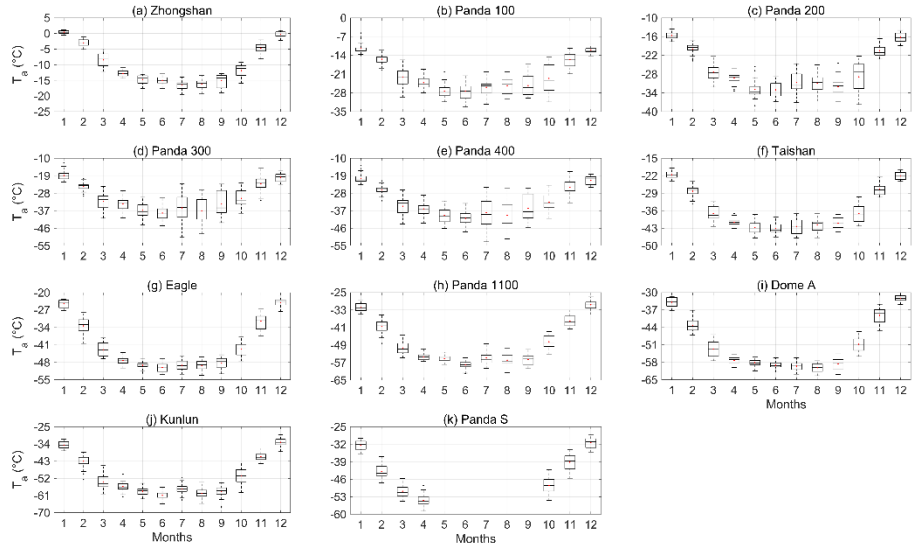
626



627

628 Figure 3. Average diurnal variation of air temperature at AWSs in the PANDA
 629 network. The calculation years for these sites are the same as for Fig. 1, excepting that
 630 Zhongshan is calculated during 2002-2020.

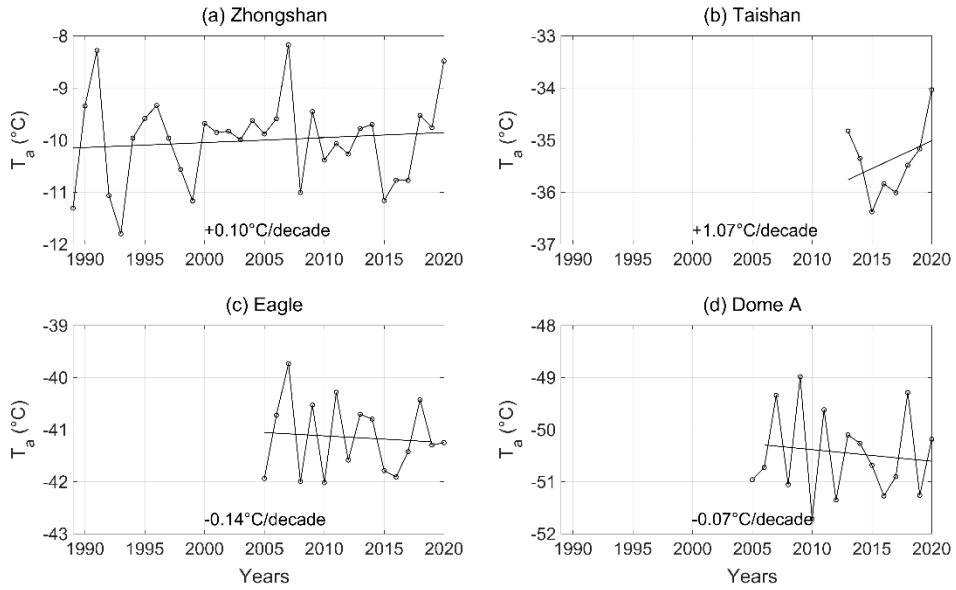
631



632

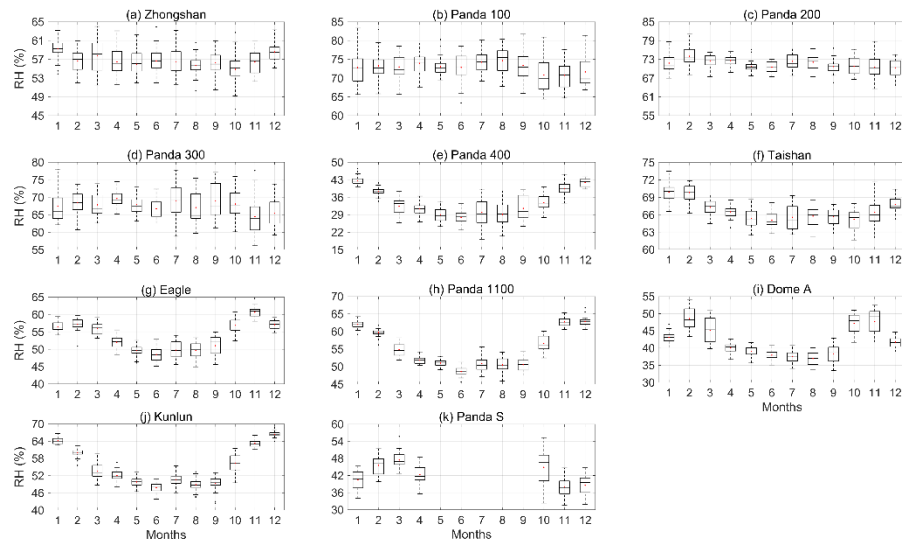
633 Figure 4. Variation of monthly mean air temperature at AWSs in the PANDA network.
 634 The calculation periods for these sites are the same as for Fig. 3, For each monthly
 635 box, the central line indicates the median, the red dot represents the mean, and the
 636 bottom and top edges of the box indicate the 25th and 75th percentiles, respectively.

637



638

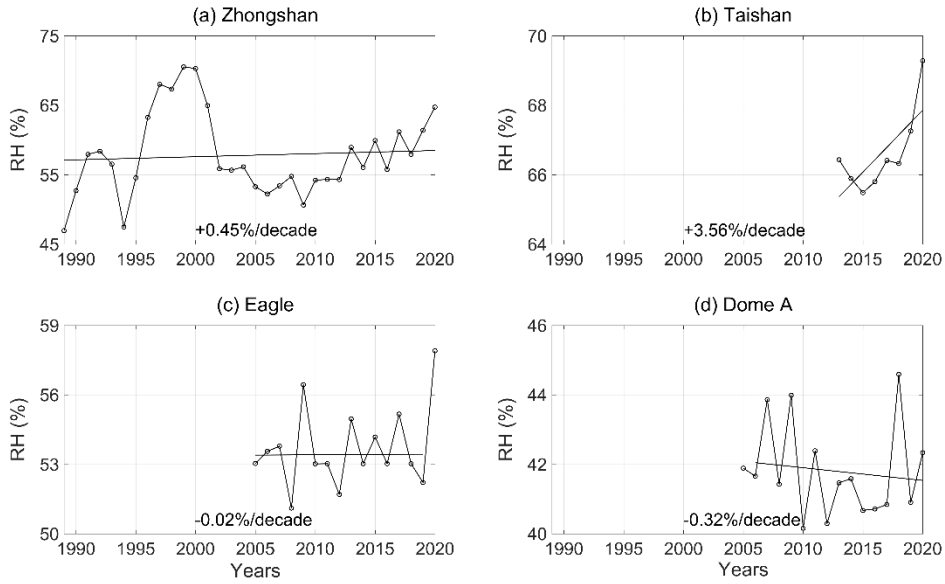
639 Figure 5. Interannual variation of air temperature at Zhongshan, Taishan ($P < 0.05$),
640 Eagle and Dome A. Zhongshan is calculated during 1989-2020; Taishan is calculated
641 during 2013-2020; Eagle and Dome A are calculated during 2005-2020.



642

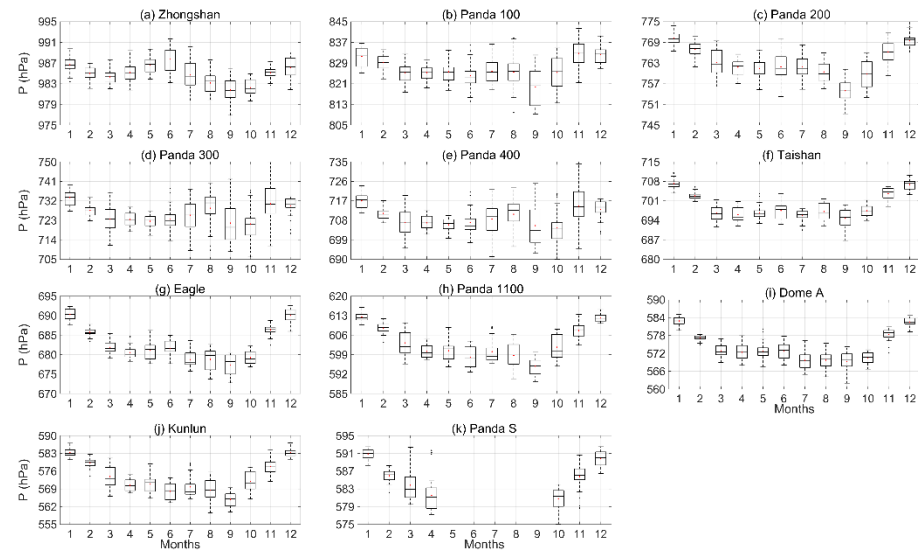
643 Figure 6. Monthly variation of relative humidity at AWSs in the PANDA network.
644 The calculation periods of these sites are the same as for Fig. 3.

645



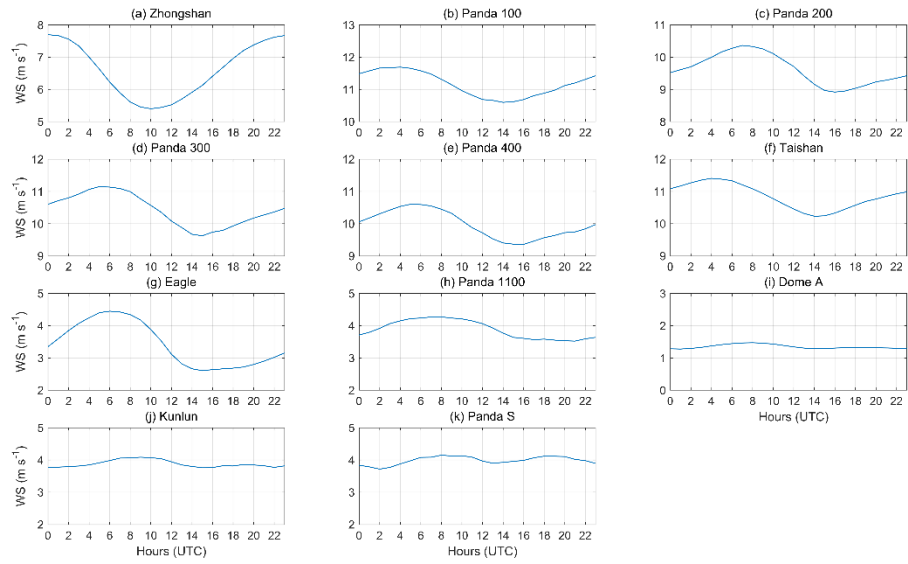
646

647 Figure 7. Interannual variation of relatively humidity at Zhongshan ($p<0.05$), Taishan
648 (p<0.05), Eagle and Dome A.



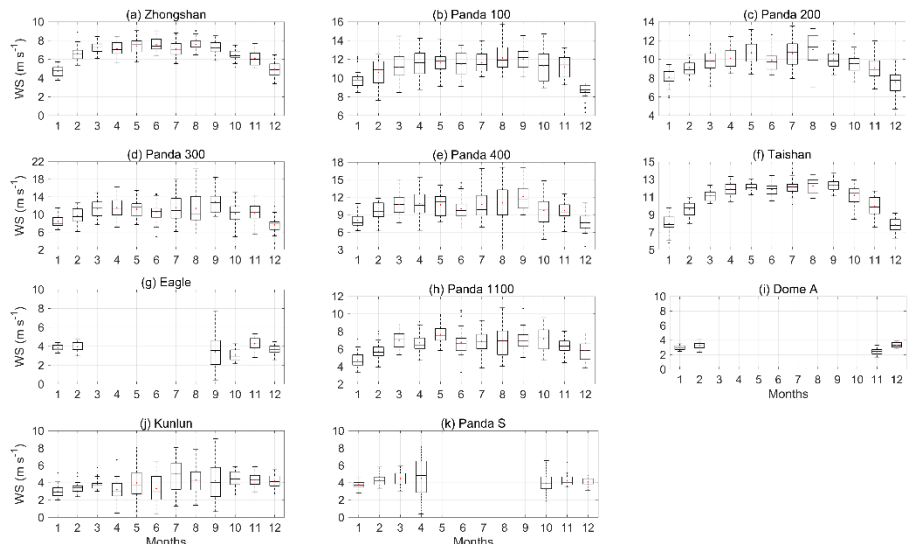
649

650 Figure 8. Monthly variation of air pressure at AWSs in the PANDA network. The
651 calculation periods at these sites are the same as for Fig. 3.



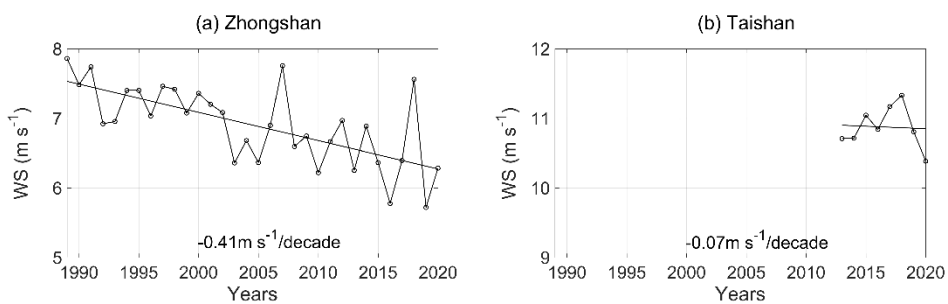
652

653 Figure 9. Diurnal variation of wind speed of PANDA AWSs network. The calculation
 654 periods of these site are the same as for Fig. 1, Zhongshan is calculated during 2002-
 655 2020.



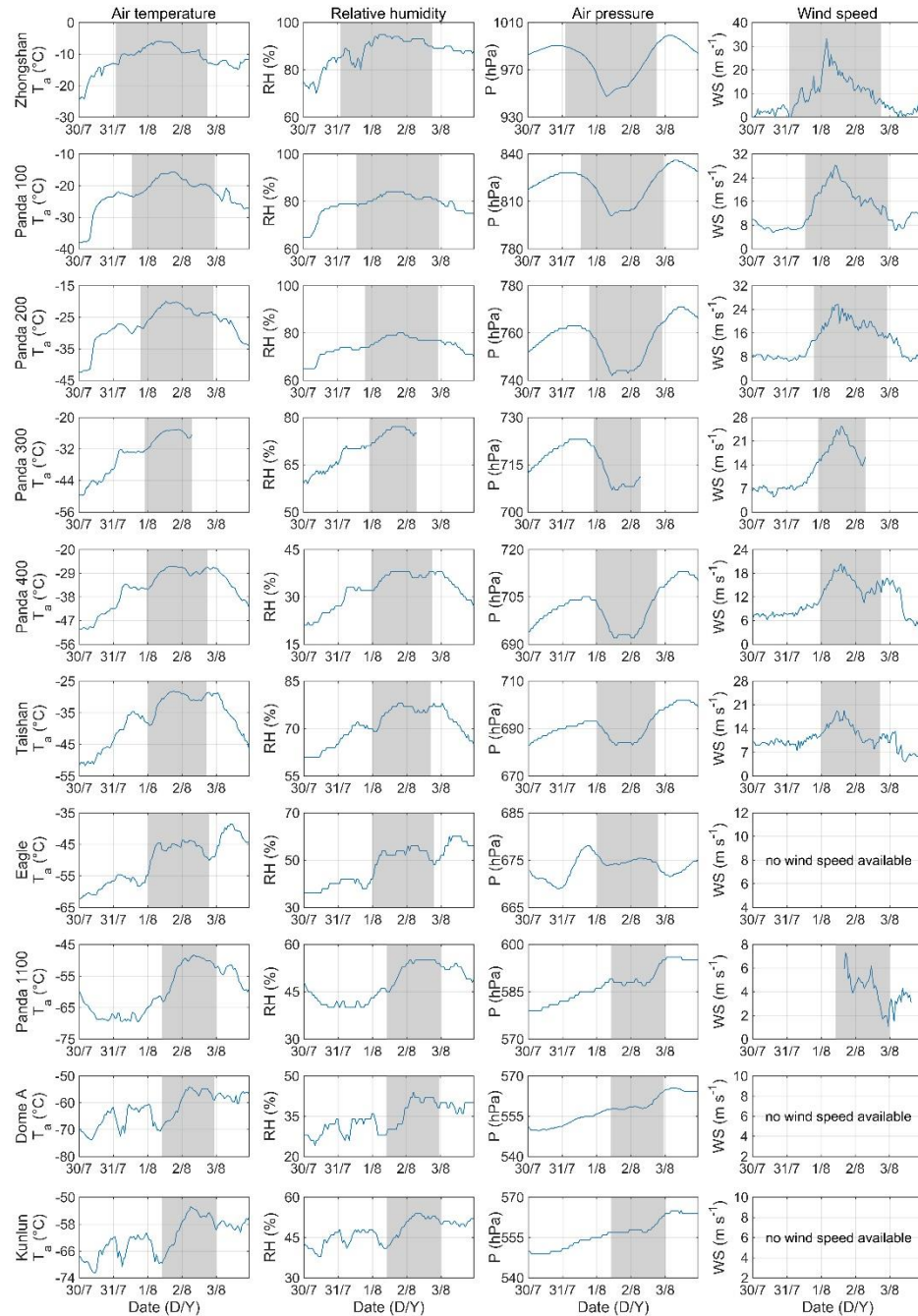
656

657 Figure 10. Monthly variation of wind speed of PANDA AWSs network. The
 658 calculation periods of these sites are the same as for Fig. 1.

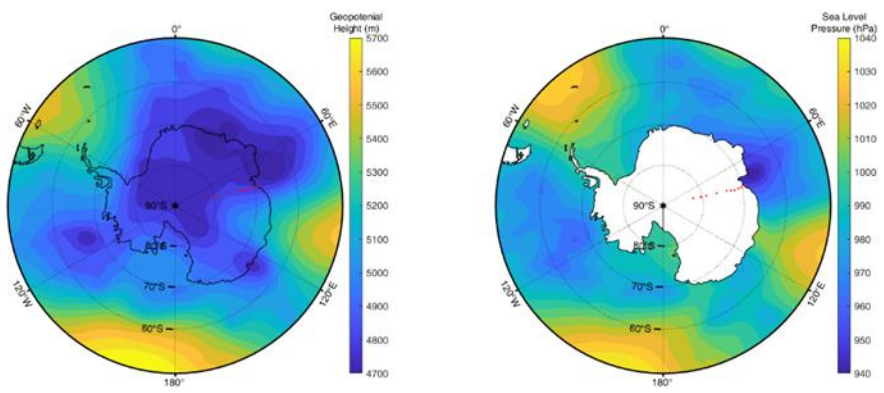


659

660 Figure 11. Annual variation of wind speed at Zhongshan (P<0.05) and Taishan
661 (P<0.05). The calculation periods of these site are the same as for Fig. 5.
662
663



664
665 Figure 12. Time series of air temperature, relative humidity, air pressure and wind
666 speed at AWS of the PANDA network (except Panda S) from 00:00 30th July to 23:00
667 3rd August 2020 (UTC); gray zone: blocking event.
668



669

670 Figure 13. The mean 500 hPa geopotential height (left) and sea level pressure (right)
 671 on 12:00 1st August (red dot: surface weather station).

672

Table 1. Locations, operational periods, observed variables and heights, and
673 instrumentation and accuracies of AWSs in the PANDA network

Station s	Locati on	Altitud e	Period (DDMMYYYYY/M)	Variabl e	Sensor	Accura cy	Height
					Vaisala		
					HMP15		
					5	(0.2260	
						-	
				Ta/RH	Campb	0028*T a) °C/1	2m
					ell		
				P	CS106	%	2m
				WS [‡]	Huayun	1.5hPa	10m
				WD	XFY3-	1m	<u>10m</u>
					1	s ⁻¹ / <u>5°</u>	
						<u>Huayun</u>	<u>5°</u>
						<u>XFY3-</u>	
						<u>1</u>	
				Ta/RH	Vaisala		2/4m
					HMP15		
					5	(0.2260	
				P		2m	
				WS			2/4m
				AWD	Vaisala	0028*T a) °C/1	<u>2/4m</u>
				SDR/S	PTB11	%	<u>2m</u>
				UR	0		
						0.3hPa	
						1m s ⁻¹ [‡]	
						5°	
						<u>5%</u>	
						<u>Max/3</u>	
						<u>%</u>	
						<u>1</u>	
						<u>Li-Cor</u>	<u>Typical</u>
				Ta/RH	Vaisala	(0.2260	4/6m
					HMP15	-	
				P	5	0028*T	4m
				WS [‡]		a) °C/1	<u>4/64/6</u>
				WD	Vaisala	%	m
				SDR/S	PTB21	0.5hPa	<u>4/6m</u>
				UR	0	1m s ⁻¹ [‡]	<u>4m</u>
						5°	
						<u>5%</u>	
						<u>Max/3</u>	
						<u>%</u>	
						<u>XFY3-</u>	<u>Typical</u>

				<u>1</u>
				<u>Li-Cor</u>
				<u>Li200X</u>
				Ta/RH Vaisala 2/4m
				HMP15 (0.2260 2/4m
			P 5 - 2/4m	
			WS [‡] 0028*T 2/4m	
			WD Vaisala a) °C/1 2/4m	
			SDR/S PTB21 % 2m	
			UR 0 0.5hPa	
			Huayun 1m s ⁻¹ [‡]	
			XFY3- 5°	
			1 5%	
			Huayun Max/3	
			XFY3- %	
			1 Typical	
			Li-Cor	
			Li200X	
				Ta/RH Vaisala 1/2/4m
				HMP15
			P 5 (0.2260 2m	
			WS [‡] - 1/2/4m	
			WD Vaisala 0028*T 1/2/4m	
			SDR/S PTB21 2m	
			URLD a) °C/1	
			0 %	
			R/LUR Huayun 0.5hPa	
			XFY3- 5°	
			Ts 1 1m s ⁻¹ [‡]	
			Tg Huayun 0.05/0.	
			XFY3- 5°	
			1 1/0.2/0.	
			Li-Cor 5%	
			Li200X Max/3	
			1 %	
			Li-Cor Typical	
			Li200X 0.2°C	
			1 0.6°C	
			Campb	
			ell Sl-	
			111	
			Campb	
			ell 109	
				Ta/RH Vaisala (0.2260 2/4m
				HMP15 -
			P 5 0028*T 2m	
			WS [‡] a) °C/1 2/4m	
			WD Vaisala % 2/4m	

			<u>SDR/S</u>	PTB11	0.3hPa	<u>2m</u>
			<u>UR</u>	0	$1\text{m s}^{-1}\textcolor{red}{f}$	
			<u>Ts</u>	<u>Huayun</u>	5°	<u>0.1/0.4</u>
			<u>Tg</u>	<u>XFY3-</u>	10%	<u>m</u>
				<u>1</u>	0.2°C	
				<u>Huayun</u>	0.6°C	
				<u>XFY3-</u>		
				<u>1Huayu</u>		
				<u>#</u>		
				<u>XFY3-</u>		
				<u>+</u>		
				<u>Campb</u>		
				<u>ell</u>		
				<u>CNR4</u>		
				<u>Campb</u>		
				<u>ell Sl-</u>		
				<u>111</u>		
				<u>Campb</u>		
				<u>ell 109</u>		
					FS23D	
					Vaisala	<u>0.0502°</u>
					HMP35	<u>C°E</u>
			Ta	D	2% <u>(RH)</u>	1/2/4m
			RH	Parosci	<u><90%)</u>	2m
			P	entific	0.5hPa	2m
				6015A		
				WS <u>AW</u>	RM	
					Young	1/2/4m
					0.5m	
					12170C	$\text{s}^{-1}\textcolor{red}{f}6^\circ$
						<u>1/2/4m</u>
						<u>0.1/1/3/</u>
					Tg	<u>Aander</u>
						<u>6°</u>
						<u>10m</u>
						<u>aa</u>
						<u>0.02°C</u>
						3590B
						FS23D
				Ta/RH	Vaisala	(0.2260
						2/4m
					HMP15	-
					P	5
					0028*T	2m
					WS <u>f</u>	$\text{a)}^\circ\text{C}/1$
					WD	Vaisala
						%
					SDR/S	PTB21
						0.5hPa
					UR	$0\text{m s}^{-1}\textcolor{red}{f}$
						Huayun
						5°

<u>Li200X</u>				
		Ta	<u>Vaisala</u>	<u>(0.2260</u>
			<u>HMP15</u>	<u>4m</u>
			<u>5PRT</u>	<u>0028*T</u>
		RH	<u>2-wire</u>	<u>a) °C</u>
		P	<u>Bridge</u>	<u>1%0.5°</u>
			<u>€</u>	<u>4m</u>
		WS <u>AW</u>	Vaisala	<u>5%</u>
		<u>D</u>	<u>HMP35</u>	<u>0.2hPa</u>
		<u>WD</u>	<u>AHMP</u>	<u>1hPa</u>
			<u>155</u>	<u>p</u>
	82.33°			<u>Campb</u>
Panda	S	4027	<u>2008/0415 Jan 2008-</u>	<u>0.21+0.</u>
S	75.99°	m a.s.l.	<u>2021/0430 Apr 2021</u>	<u>ell</u>
		E		<u>5m s⁻¹</u>
				<u>CSares</u>
				<u>35°</u>
				<u>cientifi</u>
				<u>e215</u>
				<u>A106</u>
				<u>Huayun</u>
				<u>RM</u>
				<u>Young/</u>
				<u>40K</u>
				<u>Ohmpe</u>
				<u>tXFY3-</u>
				<u>1</u>
				<u>Huayun</u>
				<u>XFY3-</u>
				<u>1</u>
674				
675	<u>Statement: SDR: downward shortwave radiation; SUR: upward shortwave radiation;</u>			
676	<u>LDR: downward longwave radiation; LUR: upward longwave radiation.</u>			
677				

678
 679
 680 Table 2 The mean values of meteorological variables on AWSs in the PANDA
 681 network

682 Stations\ 683 elements	684 Air 685 temperature /°C	686 Relative 687 humidity/%	688 Pressure 689 /hPa	690 Wind 691 speed 692 /m s ⁻¹	693 Number 694 of 695 hourly 696 values
Zhongshan	-10.0	58	985	6.9	184695
Panda 100	-21.6	73	827	11.2	21216
Panda 200	-26.5	72	763	10.9	40010
Panda 300	-30.0	68	726	10.4	13811
Panda 400	-32.0	34	710	10.0	13783
Taishan	-35.4	67	699	10.9	74893
Eagle	-41.2	54	683	3.6	139608
Panda 1100	-47.7	55	603	3.6	39648
Dome A	-50.5	42	575	2.9	140484
Kunlun	-50.8	55	574	3.9	39515
Panda-S	-	-	-	-	-